Hydration layer dynamics and association mechanisms of food and antifreeze proteins

A Molecular Dynamics and Transition Path Sampling study

Brotzakis, Z.F.

Publication date
2017

Document Version
Other version

License
Other

Chapter 3

Dynamics of hydration water around native and misfolded α-lactalbumin

As water is an essential ingredient in protein structure, dynamics and functioning, knowledge of its behavior near proteins is crucial. We investigate water dynamics around bovine α-lactalbumin by combining molecular dynamics simulations with polarization resolved femtosecond infrared (fs-IR) spectroscopy. We identify slowly reorienting surface waters and establish their hydrogen-bond lifetime and dynamical orientation relaxation dynamics, which we compare to the experimentally measured anisotropy decay. The calculated number of slow surface waters is in reasonable agreement with the results of fs-IR experiments. Slow waters form fewer hydrogen bonds compared to the bulk. At concave sites the protein-water hydrogen bonds break preferably via translational diffusion rather than via a hydrogen-bond jump mechanism. The reorientation of water molecules residing at these concave sites is slower than at convex water exposed sites. Protein misfolding leads to an increased exposure of hydrophobic groups, inducing relatively faster surface water dynamics. Nevertheless, the larger exposed surface slows down a larger amount of water. While for a native protein hydrating water is slower near hydrophobic residues than at hydrophilic sites, mainly due to stronger confinement, misfolding causes hydrophobic water to reorient relatively faster because the exposure of hydrophobic groups destroys concave protein cavities with a large excluded volume.

3.1 Introduction

The protein hydration shell is very significant and essential to protein structure, dynamics and function. The hydration shell dynamics relates to biochemical processes such as protein folding, molecular recognition and enzyme function[1–3].

Both experimental [3, 4] and simulation findings [5–7] agree on that a protein perturbs the water dynamics in its hydration shell. However, the root and the degree of this perturbation is not completely understood. Experimental techniques such as time-resolved fluorescence and NMR indicate a slowdown of water molecules close to the protein surface. NMR experiments [8], and molecular dynamics (MD) simulations[5, 7], show that most of the hydration shell water reorients 2-3 times slower compared to bulk water. The origin of this slowdown has been mostly attributed to the excluded volume effect due to topology and to a lesser extent to the strength of the hydrogen bond [5, 7].

Moreover, MD simulations [7] indicated that increasing the excluded volume and decreasing the hydration level by adding hexane molecules at the surface, led to shifted and broader reorientation time distributions. The effect of confinement on water dynamics has been assessed experimentally by polarization-resolved femtosecond infrared spectroscopy [9, 10], which showed that water near the surface of a (reversed) micelle is slow, while water in the core behaves very similar to bulk water. These experiments showed that confinement affects the dynamics of water, but only on very small length scales (sub nanometer), i.e. close to a surface. Femtosecond 2D infrared spectroscopy combined with polarization-resolved femtosecond infrared spectroscopy[11] showed that the slow component of water reorientation dynamics scales with the slow translational diffusion, indicating slow hydrogen bond dynamics near hydrophobic groups. Interestingly, in a MD study on a amyloidgenic $\alpha\beta$-disordered protein at room temperature, Jose *et al.* [12] found that water molecules around the protein exhibit faster reorientation and translation dynamics compared to water hydrating a native globular ubiquitin in water. Further studies conducted by Rahaman et al[13] observed also an acceleration of water dynamics around a temperature induced-unfolded thermophile protein compared to a folded one. Temperature induced unfolding or misfolding of the proteins alters the amount of confined water, and changes the hydrophobic/hydrophilic nature of the protein surface. The influence of this temperature induced misfolding on the water dynamics remains not well understood. In this work, by combining molecular dynamics simulations with infrared spectroscopy, we investigate the dynamics of water around the protein surface of α-lactalbumin, a major constituent of whey, and an important protein in the food industry[14]. As α-lactalbumin is a small (14 kDa) globular protein that is structurally quite similar to the widely studied

lysozyme [15], it forms an excellent system to study water dynamics in the protein hydration shell. We conducted MD simulations of several solvated α-lactalbumin systems at ambient conditions. For a native solvated protein, we conducted two different concentrations and two different water models. For a misfolded solvated protein we conducted one concentration and one water model. In addition, we measured the water reorientation dynamics using polarization-resolved femtosecond infrared spectroscopy. The remainder of the paper is organized as follows. Section 3.2 describes the employed simulation, analysis and experimental methodology. In section 3.3 we present and discuss the analysis results, and compare to the experiments. We end with conclusions in section 3.4.

3.2 Methods

3.2.1 Simulation setup

All molecular dynamics simulations were performed with the Gromacs 4.5.4 package [16]. The bovine α-lactalbumin monomer structure, extracted from the PDB 1F6S [17] was solvated with water molecules (SPC/E or TIP4P/2005), resulting in dilute solutions of approximately 5 % w/w and more concentrated solutions of 8.5% w/w (denoted 5% SPC/E, 5% TIP4P/2005, 8.5% SPC/E and 8.5% TIP4P/2005 system, respectively).

The atomic interactions were defined by the amber99sb-ildn force field [18]. The protonation state of the amino acids corresponds to pH of 7, and five Na atoms were added to neutralize the system (pkI= 4-5). For each water force-field, after energy minimization, the system was equilibrated for 1 ns at ambient conditions (298 K and 1 atm) in the NPT ensemble. All bonds were constrained with the Lincs algorithm. A cutoff of 1 nm was used for the non-bonded Lennard-Jones interactions. The Particle Mesh Ewald method was used to calculate the electrostatic interactions with a Fourier spacing of 0.12 nm and a 1 nm cutoff for the short range electrostatic interactions. Neighbor lists were updated every 10 fs with a cutoff of 1 nm and the time step was 2 fs [18]. The leap-frog algorithm was used for integrating Newton's equations of motion. In the NPT simulations the v-rescale thermostat[19] with a coupling time constant of 0.2 ps controlled the temperature, while the Parrinello-Rahman barostat[20] with a coupling time constant of 1.0 ps kept the pressure constant. From a 100 ns long MD trajectory in the NPT ensemble at ambient conditions (298 K and 1 atm) 10 frames were randomly selected from different parts of the trajectory. From each frame we initiated a short 1 ns production run in the NVE ensemble, by switching off the thermostat and barostat. This approach eliminated any unwanted influence from the thermostat or

barostat on the dynamics. To prevent energy drift we used a switching function for the non-bonded interactions from 0.8 -1.0 nm. The pair lists were updated every 5 fs with a cutoff of 1.2 nm and the time step was 1 fs. The frequency of the energy calculation was 10 fs, and the frames were saved every 100 fs in order to obtain sufficient data for the analysis.

The effect of protein misfolding on the water dynamics was investigated by analyzing two types of quenched high temperature systems. Starting from the last frame of the 100 ns ambient condition MD trajectories (for the 5% w/w SPC/E system), we ran another 100 ns at high temperature (700 K) followed by two types of quenching procedures. In the first, five high temperature frames were selected and relaxed at 298 K temperature (NPT) for 10 ns. Then, for each of these five room temperature MD runs, a frame corresponding to the average temperature, energy, and volume was selected and used to initiated a 1 ns NVE simulation for analysis, using the high frequency frame saving. This system is labelled *misfolded #1*. In the second procedure one frame corresponding to the average temperature and energy was selected from the high temperature run. Using this as an initial frame, a 100 ns simulation was performed at room temperature using a NPT simulation. From this simulation ten frames corresponding to the average energy and temperature and volume were selected, and from each, a 1 ns NVE run was conducted. This system is labelled *misfolded #2*. The ten 1 ns trajectories were subjected to dynamical analysis. We studied the misfolded protein at ambient conditions rather than elevated temperature where the unfolding occurs, in order to keep the bulk water behaviour as close as possible to the native state simulations, and focus entirely on the differences in dynamics induced by the altered protein surface.

3.2.2 Analysis

Hydrogen bond life times

For the rest of the chapter hydrogen bonds will be referred to measured as H-bonds. A H-bond was defined present if the distance between H-bond donor D and acceptor atom A, $R_{DA} \leq 0.35$ nm, and the angle between the DH and HA vectors $\theta_{ADH} \leq 30^\circ$ [21, 22]. Here, either the donor and acceptor atom can belong to the protein or to water. The H-bond lifetime was defined as the time it takes for the bond to break and to form a stable bond with another acceptor (exchange), or to remain dangling (translational diffusion). If the bond reforms within 200 fs, it is considered not broken, in order to avoid counting fast recrossings events.

The recrossing time $\Delta\tau$ = 200 fs was based on the fact that the vibrational characteristics of the water water H-bond occur in the far infrared and around 200 cm^{-1}=166

fs [23, 24]. Different values of this recrossing time $\Delta\tau$ = 0 fs and $\Delta\tau$ = 400 fs were used to test whether this choice affects the results.

Water reorientation dynamics

Reorientation dynamics can be represented using the time correlation function [25, 26]

$$C_2(t) = \frac{2}{5}\langle P_2[\mathbf{u}(0)\cdot\mathbf{u}(t)]\rangle \tag{3.1}$$

where P_2 denotes the second Legendre polynomial, $\mathbf{u}$ is the unit vector characterizing the orientation of an OH group in a given frame and the angular brackets denote an ensemble average over all water molecules and all time origins. This correlation function can easily be related to anisotropy curves obtained from polarization-resolved femtosecond infrared spectroscopy and to orientation relaxation times from magnetic relaxation techniques [25].

From MD simulations we compute the reorientation dynamics for each individual molecule. We are particularly interested in the anisotropy decay of water molecules hydrating different protein sites. The reorientation dynamics of individual water molecules was investigated by following the dynamics of both OH bond vectors of each molecule j. For each bond unit vector $\mathbf{u}_{jk}(t)$, we computed the time correlation function

$$c_j^m(t) = \frac{1}{5\ell}\sum_{t'=t_0^m}^{t_0^m+\ell\Delta t}\sum_{k=1}^{2} P_2[\mathbf{u}_{jk}(t'))\cdot\mathbf{u}_{jk}(t'+t))] \tag{3.2}$$

where the sum over $k = 1,2$ refers to the two OH bond vectors, and the time correlation is summed over the mth time interval $t_0^m < t' < t_0^m + \ell\Delta t$ that the molecule is within the hydration layer of the protein (defined as the water oxygen being within 4.4 from the protein heavy atoms). We used a buffer time of 2 ps to avoid counting fast non-essential excursions inside and outside the hydration layer [27]. For each curve $c_j^m(t)$ we extracted the reorientation decay time τ_j^m by fitting $c_j^m(t)$ to a single exponential fit in the interval $0 < t < 10$ ps (see Fig. 3.A.3). Each estimate m was viewed as a separate measurement, since the water molecule can change its dynamics when leaving or entering the hydration layer. For each water molecule j and for each mth interval of length ℓ the decay time τ_j^m was histogrammed with a weight ℓ, leading to a probability distribution of decay times. The weight ℓ follows from the fact that the correlation in eq. 3.2 occurs ℓ times in eq. 3.1. The average decay time τ from these histograms thus should be close to the overall decay time of eq.3.1. The decay times of the individual water molecules allow us to establish the relation between the water structure and dynamics. We therefore divide the waters into several categories.

For each water molecule j and for each mth interval ℓ the decay time τ_j^m was histogrammed with a weight ℓf_{HB} in the protein H-bonded category or with a weight ℓf_{nHB} to the category of water that is non H-bonded to the protein. Here f_{HB} and f_{nHB} refer to the fraction of frames in the interval ℓ in which the water j was hydrogen bonded to the protein or not.

A similar procedure was followed for categorizing and histogramming hydrophobic or hydrophilic water. For each water molecule j, the decay time τ_j^m for each mth interval ℓ was histogrammed with a weight ℓf_{HP} and ℓf_{HF} for hydrophobic and hydrophilic water, respectively. Here f_{HP} and f_{HF} are the fraction of frames in the interval ℓ in which the water j solvated respectively, a hydrophobic and hydrophilic group (i.e. the water oxygen was within 4.4 of, respectively an apolar or polar residue side chain).

In both cases the sub-population histograms add up to the total probability histograms. Errors in the mean were estimated from block averaging.

3.2.3 Polarisation-resolved femtosecond infrared spectroscopy

Experimentally, we measured the water reorientation dynamics using polarization-resolved femtosecond infrared spectroscopy [9–11, 24, 28–30]. Protein solutions were prepared by mixing bovine $\alpha-$lactalbumin (purity $> 90\%$, Davisco foods) with isotopically diluted water, consisting of ultrapure milli$-$Q grade H_2O and 4% D2O (99.9 %D, Cambridge Isotope Laboratories). The deuterated hydroxyl (OD) groups in this solution absorb strongly at 2500 cm^{-1}, which corresponds to the stretch vibration of the OD group.

We excited and probed the OD stretch vibrations using resonant infrared pulses. These pulses were generated by frequency conversion of the output of a Ti:sapphire regenerative amplifier that produces 850 μJ, 100 femtosecond pulses with a center wavelength of 800 nm at a repetition rate of 1 kHz. Part of the light was used to pump a BBO$-$based optical parametric amplifier. The 2 μm idler pulses produced by this amplifier were frequency$-$doubled in another BBO crystal and subsequently mixed with the remaining 800 nm light in a lithiumniobate crystal, yielding 10 μJ pulses at 2500 cm^{-1}, with a pulse duration of 200 fs and a bandwidth of 100 cm^{-1}. These pulses were separated into pump, probe and reference beams by a wedged CaF_2 window and focused onto the sample by a parabolic mirror. The sample consisted of the protein solution sandwiched between two CaF_2 windows, held apart by a 50 μm spacer. After passing through the sample, the probe and reference beams were recollimated by a second parabolic mirror, dispersed in a grating-based spectrometer and detected with two lines of a 3x32 mercury$-$cadmium$-$telluride detector array.

The pump pulse induced transient absorption changes in the sample that we monitored with the probe pulse (the reference pulse was used for normalization to correct

for pulse to pulse fluctuations of the infrared light). We measured the transient absorption for probe pulses with their polarization parallel and perpendicular with respect to the pump polarization. Since the pump pulse most efficiently excites OD vibrations with their transition dipole moment parallel to the polarization direction of the light, initially the parallel absorption signal is higher, while after some time the orientation of the OD stretch vibration has randomized and the parallel and perpendicular signals become equal. From the parallel ($\alpha_{(\parallel)}$) and perpendicular ($\alpha_{\perp}$) transient absorption signals we constructed the anisotropy:

$$C_2(v,t) = \frac{\alpha_{(\parallel)}(v,t) - \alpha_{(\perp)}(v,t)}{(\alpha_{(\parallel)}(v,t) + 2\alpha_{(\perp)}(v,t))} \tag{3.3}$$

The anisotropy C_2 of eq. 3.3 decays with the rate of molecular reorientation and is directly proportional to the second-order reorientation correlation function shown in equation 1.

Table 3.2.1: Simulation: Average protein water and bulk water H-bond lifetimes for six different systems 1) 5% protein in SPC/E water 2) 8.5% protein in SPC/E water 3) misfolded #1 4) misfolded #2 5) 5% protein in TIP4P/2005 water 6) 8.5% protein in TIP4P/2005 water. The number subscript indicates the error in the last digit.

system #	1	2	3	4	5	6
t_{bulk}	2.45_1	2.47_1	2.45_1	2.47_1	2.90_1	2.95_1
t_D	3.27_5	3.41_{13}	3.43_7	3.61_{15}	3.93_5	3.84_5
t_A	4.62_9	4.70_{14}	4.53_{15}	4.67_{13}	5.72_{10}	5.61_{21}
t_{D+A}	3.99_6	4.23_{14}	4.01_{14}	4.17_{14}	4.84_7	4.74_7
$t_{directD}$	1.99_5	1.53_5	2.15_2	2.14_5	1.97_5	1.88_3
S_{HB}	1.62	1.71	1.63	1.69	1.67	1.60

3.3 Results and Discussion

3.3.1 Hydrogen bond dynamics

The computed H-bond life times for the six studied systems are shown in Table 3.2.1. The average and standard deviation is taken from a block average of 10 sets of data per system. While the H-bond lifetime is sensitive to the selected recrossing time, the H-bond lifetimes follow the same trend when using different recrossing time $\Delta\tau$ [31]. We

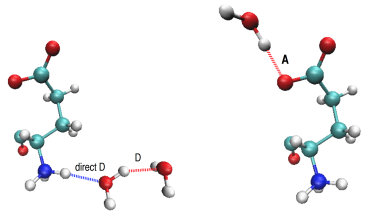

Figure 3.3.1: Representation of the H-bond type. Left: a protein donating a H-bond to water, labelled directD and the accepting water donating a H-bond to another water labelled D. Right: a protein accepting a H-bond from water, labelled A. The classification includes both backbone and side-chain H-bonds.

distinguish between water molecules that are H-bonded to other water molecules in the bulk, and water molecules that are donating or accepting H-bonds from the protein, as illustrated in Fig. 3.3.1. A protein H-bond donor leads in fact to two types of H-bonds, labelled the directD and D, with the first one being more informative about the direct protein water interaction and the second one giving more relevant information on the reorientation of the OH vectors of the water accepting a H-bond from a protein donor (see Fig. 3.3.1 left). The H-bond type when the protein is accepting a hydrogen from water is labelled A (see Fig. 3.3.1 right). Table 3.2.1 shows that the overall average protein-water H-bond lifetime (t_{D+A}) is always longer than the H-bond lifetime in bulk water (t_{bulk}) for all systems in this study, mainly due to bonds between accepting protein groups and water (t_A). The relative increase of the protein-water H-bond lifetimes at the protein surface can be expressed as the ratio S_{HB} of the average protein-water H-bond lifetime over the average lifetime in the bulk (see Table 3.2.1). The protein-water H-bond lifetime distribution is broad, including short H-bonds but also long-lived bonds, as indicated by the long tail in Fig. 3.A.1. The protein H-bond acceptors (t_A) form longer-lived bonds than the protein H-bond donating groups (t_D and $t_{directD}$), which agrees well with the work of Sterpone et al[5, 32] who showed that the water dynamics is slowed down more at protein H-bond accepting groups. Upon misfolding the protein-water H-bond lifetimes does not change much compared to the folded native state. However, the average lifetimes of H-bonds between protein donating groups and water (t_D and $t_{directD}$) increases upon misfolding, suggesting the existence of water mediated interactions between the protein residues in the misfolded systems, which are known to mediate folding of misfolded and unfolded systems [33]. Such a water mediated interaction is illustrated in Fig. 3.A.2. The H-bond dynamics in the 5% TIP4P/2005

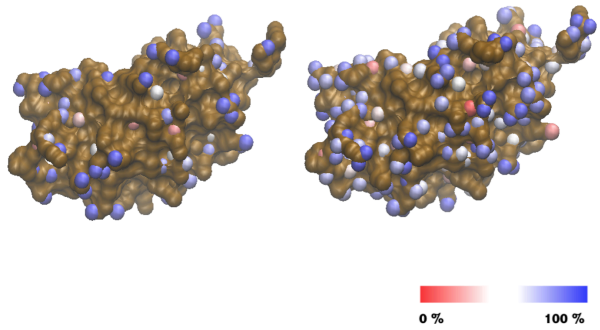

Figure 3.3.2: Simulation: Percentage of occurrence of jump mechanism of protein-water H-bond breaking projected on protein atoms. Left: type D, H-bonds. Right: type A, H-bond. Blue sites indicate that 100% of the H-bonds break via a jump mechanism, while red represents breaking through diffusion. Ochre sites do not form protein water H-bonds.

system is substantially slower compared to the 5% SPC/E system. The larger standard deviation of protein water H-bond lifetimes upon misfolding is due to the different conformations in the ten analyzed windows of the misfolded system. The effect of protein concentration on the protein-water H-bond dynamics is marginal. Note that for the SPC/E system, the protein-water H-bond dynamics slightly decelerates with concentration, whereas it slightly accelerates for the TIP4P/2005 system.

To investigate the nature of the water-protein H-bond dynamics, we analyzed the H-bond breaking mechanism as a function of the protein site. For this process, Laage et al [34] introduced a framework involving large-amplitude angular jumps upon H-bond breakage. Figure 3.3.2 depicts the percentage of protein water H-bonds breaking via jumps as a function of the protein sites. This figure clearly shows a correlation between the curvature of the protein site (excluded volume) and the mechanism of H-bond breaking. For convex protein sites, protein water H-bonds break more likely via a jump mechanism, whereas for concave sites (occurring more in buried residues) H-bonds break via translational diffusion. This finding was also reported in the work of Brandeburgo et al [24], and can be rationalized by realizing that at concave sites there is less space for new hydrogen-bond partners, making it less likely that a water OH will find a new partner to jump to through an angular jump, thus increasing the chance of H-bonds breaking via diffusion.

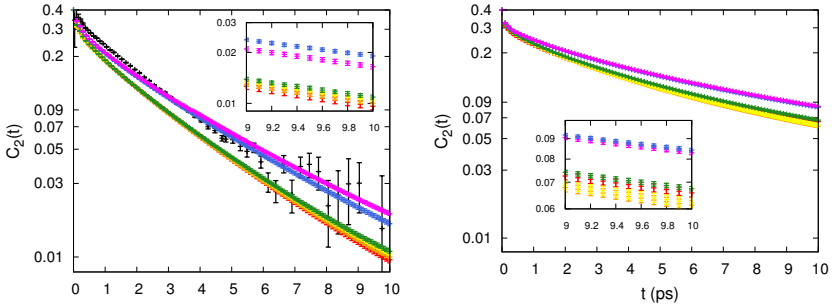

Figure 3.3.3: Simulation: Left: Logarithmic plot of the anisotropy decay of all water molecules for the six simulated systems. Right : Anisotropy decay for hydration layer only. 5% SPC/E (red), 8.5% SPC/E (dark green), misfolded #1 (orange), misfolded #2 (yellow),5% TIP4P/2005 (blue), 8.5% TIP4P/2005 (magenta). Experimental anisotropy decay for a 5%wt protein solution, averaged over the frequency range 2450-2620 cm^{-1} (black).

3.3.2 Reorientation dynamics

Anisotropy decay of water

Figure 3.3.3(left) shows for the six simulated systems the computed anisotropy decay averaged over all water molecules, as well as the experimental anisotropy decay curve for a 5% w/w protein solution, measured by polarization-resolved femtosecond infrared spectroscopy. While the computed anisotropy curves for SPC/E are systematically lower than the experimental one, their slope is very similar. As the hydration water comprises only 6% of the overall water in the simulation box, these decay curves are dominated by the reorientation time of bulk water. Fig. 3.3.3(right) shows the simulated anisotropy decay for water molecules that are initially in the hydration layer (within 4.4 Å of the protein side chain heavy atoms). In accordance with the work of Sterpone et al. and Fogarty et al. [5, 7], for all systems the decay time of the hydration shell anisotropy is longer compared to the corresponding overall water anisotropy decay of Fig. 3.3.3(left). Thus, the water reorientation dynamics in the hydration shell of the protein is slowed down for all systems under study.

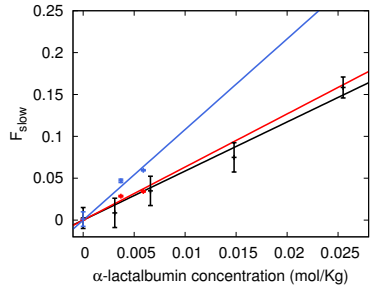

Figure 3.3.4: Simulation: Fraction of slow water molecules as a function of α-lactalbumin concentration. Blue depicts the TIP4P/2005 system, red the SPC/E system. Experiment: Black depicts the results ot the fs-IR experiments. The lines are linear fits to the data points.

Slow waters

The anisotropy decay curve can be described at intermediate times ($0.5 < t < 7$ ps) with the expression

$$C_2(t) = R_0 e^{-t/t_r} + R_1 \tag{3.4}$$

where the constant R_1 represents the water molecules in the hydration layer of the protein that reorient very slow ($t > 7$ ps), while most of the water molecules reorient with bulk-like reorientation time t_r. We limit our analysis to the first 7 ps of the anisotropy decay because the standard deviation in the ultrafast infrared experiments increases strongly with increasing delay time. Reducing the water content by increasing the concentration leaves t_r more or less constant. For the simulations t_r is 2.417 ± 0.031 and 2.40 ± 0.02 for 5% w/w SPC/E and 8.5% w/w SPC/E respectively, close to the experimental value of bulk like water t_r= 2.45 ± 0.15. The fraction of slow waters $f_{slow} = R_1/0.4$ (0.4 is the maximum value of the anisotropy) increases with the protein concentration, both in experiment and simulations. Figure 3.3.4 shows f_{slow} as a function of protein concentration. The slope of the plot of f_{slow} versus the concentration (in mol/kg water), multiplied with 55.25 (mol water molecules per kg) then yields the number of slow waters per protein molecule. The experimental data yield 323 ± 16 water molecules. For the SPC/E simulations, the number of slow water molecules is 350 ± 33. The SPC/E simulation data (bulk, 5% and 8.5%) in Fig. 3.3.4 fall within the error bars of the experimental values, and are hence in relatively good agreement with the experiment.

Analyzing the simulation results, we can also compute the amount of slow water molecules from the distribution of reorientation times as the fraction of the protein hydration shell water population reorienting slower than τ= 7 ps (see Fig. 3.3.5 right). Multiplying this fraction with the average number of hydration waters gives the number of slow water molecules (again per protein molecule since there is only one protein in the simulation box), which can again be compared with the experiment. For the 5 % SPC/E system the simulations yield 294 ± 7 slow water molecules, in fairly good agreement with the number of slow water found by experiments. The discrepancy between the two SPC/E estimates lies in the different ways of estimating the slow water content.

In contrast, for the 5% TIP4P/2005 system we find a higher number of slow water molecules compared to experimental findings. Calculating the number of slow water molecules from the slope of f_{slow} and the reorientation time distribution we find 597 ± 45 and 519 slow water molecules, respectively. The slower dynamics of TIP4P/2005, is to be expected, since Vega et al[35] report a higher reorientation time for the TIP4P/2005 bulk water compared to the SPC/E bulk water by a factor of 1.2. The SPC/E model predicts the static dielectric constant better than TIP4P/2005[35] for the bulk water, therefore, it is expected to reproduce the experiments better.

Triexponential fit of hydration water relaxation

As the experimental signal to noise ratio vanished for times larger than 7 ps and because the total anisotropy curve is dominated by bulk water relaxation, it does not make sense to fit to functions more complex than eq. 3.4 to the experimental data. However, the situation is different for the hydration layer water molecules as calculated from the simulations. As these waters are significantly slower than bulk water and experience a heterogeneous environment, it is worthwhile to fit the simulated hydration shell anisotropy decay (Fig. 3.3.3 right) to a triexponential function for times $0 < t < 70$ps:

$$C_2(t) = a_0 e^{-t/\tau_{r0}} + a_1 e^{-t/\tau_{r1}} + a_2 e^{-t/\tau_{r2}} \tag{3.5}$$

with a_0, a_1, a_2 the amplitudes of the three exponential decay modes. There are three characteristic decay times a sub picosecond (τ_{r0}) a moderate (τ_{r1}) and a slow (τ_{r2}) time scale. The sub-picosecond reorientation time is due to water libration modes, while the moderate and slow component indicate slower water reorientation mechanisms, dependent on the interaction with the protein. This observation agrees with the work of Brandeburgo et al. [24]. The relaxation times are larger for the TIP4P/2005 systems compared to the SPC/E systems, as shown in Table 3.A.1, 3.A.2 and Fig. 3.3.3. Note also that, upon misfolding, the moderate and slow characteristic time scales decrease, indicating a speed up of hydration water.

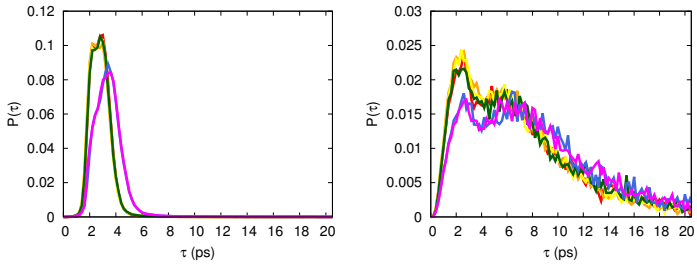

Figure 3.3.5: Simulation:probability distribution of reorientation decay τ of water molecules based on a geometrical ensemble, initially outside of the hydration shell (left) and initially in the hydration shell (right), for the six systems of study: 5% SPC/E (red), 8.5% SPC/E (dark green), misfolded #1 (orange), misfolded #2 (yellow), 5% TIP4P/2005 (blue), 8.5% TIP4P/2005 (magenta).

Distribution of reorientation times

The reorientation time of a water molecule clearly depends on its environment. This heterogeneity in the dynamics is visible in Fig. 3.3.5 which shows the probability distribution of the reorientation time τ for bulk water (Fig. 3.3.5 left) and for water molecules that are initially in the protein hydration layer (Fig. 3.3.5 right). The distribution for hydration water is much broader and extending toward longer reorientation times than the bulk water distribution (Fig. 3.3.5 left) which is roughly Gaussian, centered around 2.5 ps for SPC/E water and around 2.9 ps for TIP4P/2005 water. Note that the percentage of the hydration shell water reorienting slower than 100 ps is really small, less than 1.5 % out of the overall hydration shell water. Fig. 3.3.6 visualizes the water reorientation time as function of protein site. It can be seen that some buried residues are hydrated by very slow internal waters, whereas at the surface, the water reorientation dynamics is relatively faster. As indicated in section 3.3.1, water that is initially H-bonded to the protein at concave sites is more confined and more likely to break its bond (type A or D) through translational diffusion [24]. Due to the reduced possibility to break the H-bond via a jump mechanism through a bifurcated hydrogen-bonded transition state, these water molecules reorient on longer timescales.

Splitting the distributions

Figure 3.3.5(right) shows the probability distribution for reorientation times of the hydration layer waters. These distributions are non Gaussian due to the heterogeneous environments of the hydrating water molecules. In addition bulk-like water still con-

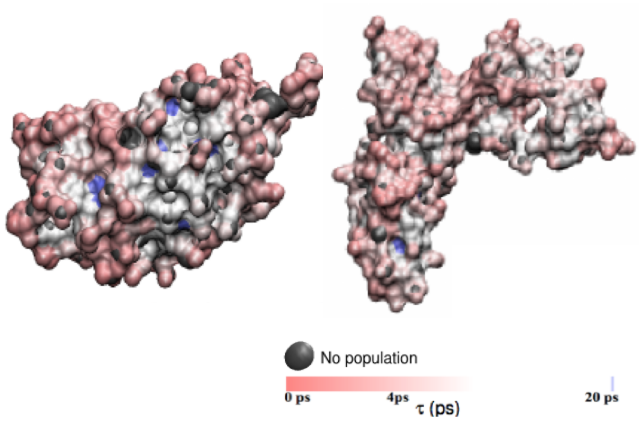

Figure 3.3.6: Simulation: The water reorientation decay times and the nature of the heavy atoms projected on protein surface for the two systems a) 5% SPC/E, (top) b) misfolded #1 (bottom). Note that the misfolded configuration has fewer blue sides, indicating relatively faster water reorientation.

tributes to this distribution due to the definition of the hydration layer, and gives a peak at 2.5 ps, the characteristic reorientation time for bulk water. To obtain more insight into the origin of the heterogeneous reorientation time distribution in the hydration layer we categorize the water molecules based on their environment. For instance, we can subdivide the hydration water populations in hydrophobic and hydrophilic waters, based on the nearest protein residue (see methods). Figure 3.3.7 (first column) and shows such. Rather surprisingly, the hydrophilic and hydrophobic distributions do not show much difference in shape. This might be due to our weighting procedure, which mixes the hydrophilic and hydrophobic categories to some extent. Table 3.A.2 reports the average reorientation time of the categories for all systems. For the native state systems, the hydrophobic water is slightly slower than hydrophilic water, possibly due to the fact that hydrophilic side groups are sightly more accessible to bulk like water.

Another way we can categorize the water molecules is in terms of H-bonding to the protein. Figure 3.3.7 (right column) shows the distributions for this division a folded and misfolded system. The water H-bonded to the protein is slower than the water that is not H-bonded to the protein. Note, that the latter category can be either

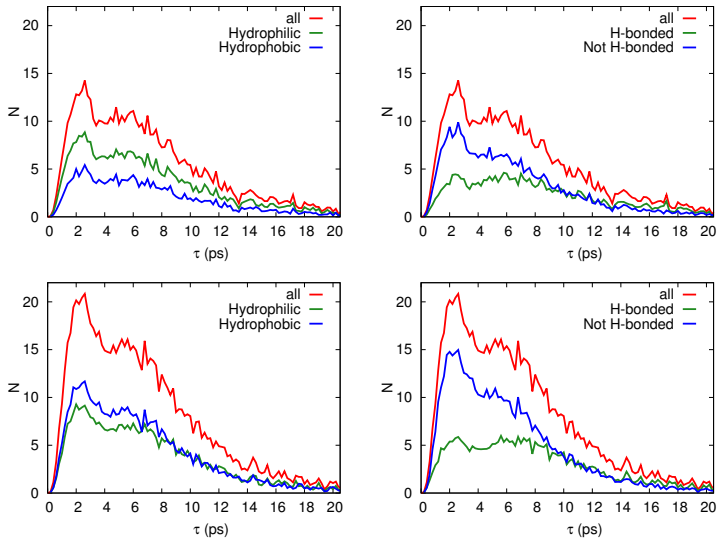

Figure 3.3.7: Simulation: Number distributions of reorientation decay times of the hydration water for 5% SPC/E (top row) and misfolded #1 (bottom row). The first column depicts the overall hydration water (red), and its subdivision into molecules hydrating hydrophilic (green) and hydrophobic (blue) groups. The second column depicts the overall hydration water, (red), and its subdivision into molecules that are H-bonded to the protein (green) and molecules that are non H-bonded to the protein(blue).

hydrophobic or hydrophilic water which is not H-bonded to the protein. The protein H-bonded water distribution exhibits a less pronounced bulk-like water peak, and has a long tail while the non protein H-bonded water has a larger contribution of bulk-like water. Table 3.A.2 shows that indeed the average reorientation time for the protein H-bonded waters (τ_{HB}) in the native state is significantly longer than for the non protein H-bonded waters (τ_{nHB}).

One can further subdivide the water molecules that are H-bonded to the protein into waters that donate their hydrogen to a protein acceptor and waters that accept a bond from a protein donor. As shown in Table 3.A.2, in all systems water donating its hydrogen to a protein acceptor (τ_{HBacc}) reorients slower compared to water that is accepting a hydrogen from a protein hydrogen donor (τ_{HBdon}). This observation is in accordance with the results of Table 3.2.1 which showed that protein H-bond acceptor (t_A) form longer-living bonds than the protein hydrogen donating groups (t_D and $t_{directD}$). We

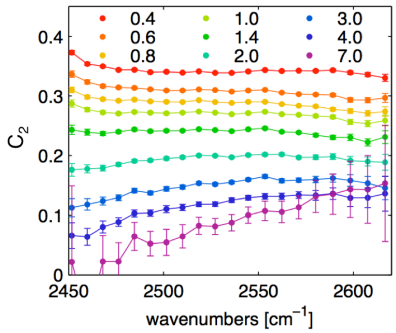

Figure 3.3.8: Experiment: Anisotropy decay for 30%w/w α-lactalbumin in isotopically diluted water as a function of frequency at different picosecond delay times.

find that the strength of the H-bond, also plays a role in the reorientation dynamics, shown also by Usui et al [36] .

The curves in Fig 3.3.7 suggests three reorientation time regimes for the surface population, a bulk like (0-4 ps) peaked at 2.5 a moderately slow (4-20 ps) and a very slow ($>$ 20ps). Therefore we can also compare the different types of water based on their distribution over these time regimes (table 3.A.3).

Table 3.A.3 shows the population of hydration shell water molecules reorienting bulk-like, moderately slow or very slow according to its category: hydrophilic (HF), hydrophobic (HP), H-bonded to the protein (HB), non H-bonded to the protein (nHB), and finally all waters (all). While the hydrophobic/hydrophilic division hardly affects the fractions, clearly the waters that are H-bonded show a significantly larger fraction in the slow category, as expected. Again, TIP4P/2005 shows a slower behavior than SPC/E. Note that upon increasing the protein concentration (reducing the bulk water) for both SPC/E and TIP4P/2005 system, the hydration shell water reorients on average the same (see Table 3.A.2).

Correlation of reorientation time with H-bond coordination number

The dynamical heterogeneity of the protein hydration water is also observable experimentally. Fig 3.3.8 shows the measured anisotropy decay as a function of frequency at different picosecond delay times. For bulk water, the anisotropy decay is independent of frequency; but for water in α-lactalbumin solutions the anisotropy decay becomes frequency dependent, with a slower decay on the high frequency side. As the

frequency of the OD vibration depends on the H-bond strength, with strong H-bonds corresponding to low OD frequencies and weak H-bonds corresponding to high OD frequencies, this plot shows that water molecules with weaker H-bonds (high frequencies) reorient slower. This frequency dependence is not observed for small amphiphilic solutes [13, 33], and therefore likely originates from the protein structure. This is consistent with the observation that the slowest reorienting waters are located in concave sites on the structured protein surface (Fig. 3.3.6). It also suggests that there is a correlation between the position of a water molecule at the protein surface and its H-bond strength. To further investigate this, we analyze the H-bond coordination in the protein solutions, which directly influences the frequency of the OD stretch vibration [37].

Recently, Auer and Skinner [37] used Raman and VSF spectroscopy experiments to classify molecules in terms of H-bond structure in bulk and at a liquid vapour interface. In particular, they classified each water molecule by its number of H-bond acceptor n_A and donors n_D. Here we adopt this classification of the H-bond structure, using a slightly different notation (n_A-n_D), where n_A is the number of accepted H-bonds, and n_D the number of donated H-bonds (see Fig. 3.3.9a for an illustration). Note that these numbers include bonds accepted from and donated to the protein. For bulk water, the population of the different H-bond classes was found to decrease in the order $(2\text{-}2) > (1\text{-}2) > (2\text{-}1) > (1\text{-}1) > (0\text{-}2)$. Our simulations show the same order for bulk water in the different protein systems (see Fig. 3.3.9 and Fig. 3.A.4). We find the average number of H-bonds of bulk water to be 3.54 and 3.62 for SPC/E 5% and 8.5%, respectively, in accordance with reported values of 3.59 for SPC/E water[38]. Fig. 3.3.9b shows that near a protein water interface, in this case for the 5% SPC/E system, the water H-bond class population decreases in the order $(2-2) > (1-2) > (2-1) > (1-1) > (0-2)$, which is the same as for bulk water. However, comparing protein hydration shell water with bulk water the populations $(1-2)$ and $(1-1)$ are enhanced and $(2-1)$ and $(2-2)$ are reduced in the hydration shell. This shift leads to an average of 3.31 H-bonds for the hydration shell water, which is less compared to bulk water (3.59 H-bonds). Similar results are found for the 5 % TIP4P/2005, misfolded #1 and misfolded #2 systems with average H-bond numbers of 3.43, 3.29 and 3.29, respectively.

To relate the contribution from each of the H-bond classes to the water reorientation time distributions we partitioned these distributions based on the coordination labels (n_A-n_D). The resulting distributions are shown in Fig. 3.3.9c and Figs. 3.A.5 to 3.A.10.

The H-bond class of a water molecule does not seem to have a dramatic effect on the reorientation time distribution. To see the difference more clearly in Fig. 3.3.9d we separate for the 5% SPC/E system the distributions for the different populations into three reorientation time regimes: a bulk like (0-4 ps) peaked at 2.5, a moderately slow (4-20 ps) and a very slow ($>$ 20ps). Even though the populations themselves

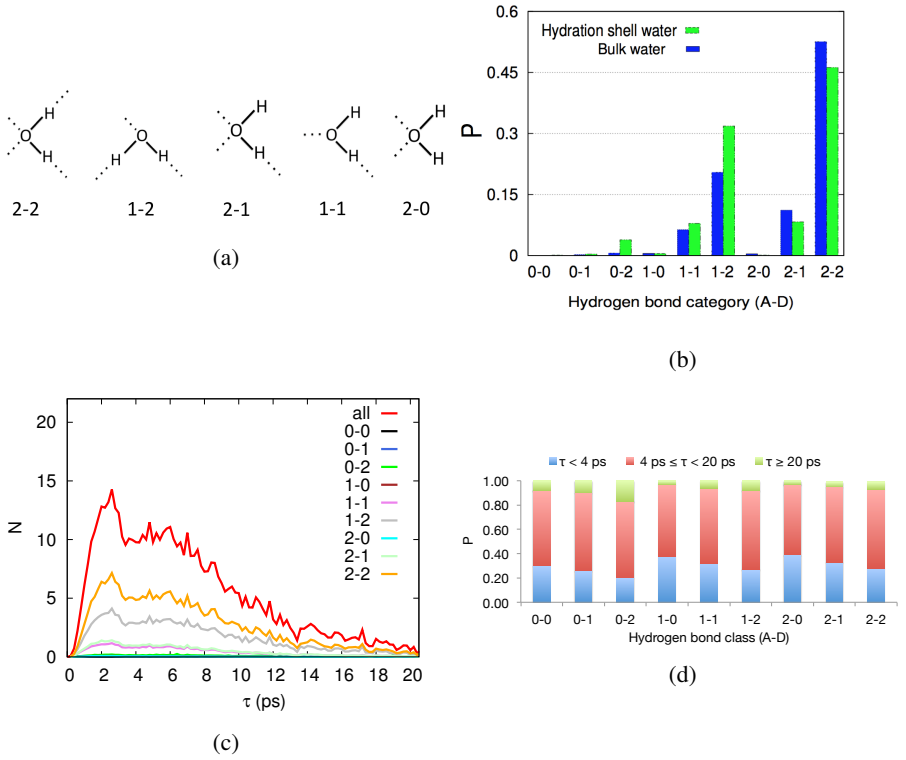

Figure 3.3.9: Simulation: a) illustration of H-bond classes b) populations of each H-bond class, subdivided into bulk and hydration shell water (for the 5% SPC/E system). c) Number distribution of the reorientation decay times of hydration shell water for the different H-bond classes (for the 5% SPC/E system). d) Percentage of water reorienting in the bulk-like (blue), moderate (red) and slow (green) regime for the different H-bond classes (for the 5% SPC/E system).

are widely spread, there is a clear correlation in this table: water with more donated H-bonds are slower, waters with more accepted H-bonds faster (increased bulk like population). This pattern occurs in all hydration water, but not in bulk, where there is no correlation between the water structures and the dynamics. This correlation is made even clearer in Table 3.A.4 which shows the fraction of water as a function of number of donated and accepted H-bonds, irrespective of class. The correlation however, does

not mean causation. Much more likely, the presence of the surface induces both effects: fewer accepted H-bonds, and slower reorientation dynamics.

Effect of misfolding on reorientation dynamics

There seems to be a negligible difference between the two types of misfolded systems in terms of the reorientation decay times, as the average τ values given in Table 3.A.2 are similar and the anisotropy decay curves in Fig. 3.3.3 are identical within the error. However, the hydration shell water reorientation time is faster compared to the native structure (see Table 3.A.1, 3.A.2 and Fig. 3.3.3right). This is in accordance with the work of Jose et al [12] who showed that the disordered Aβ_{1-42} amyloid protein exhibits faster water reorientation dynamics than a globular ubiquitin protein.

From the distributions of Fig. 3.3.7 and Fig. 3.A.8, the calculated number of slow water molecules for the misfolded systems are 373 and 401 for misfolded #1 and misfolded #2, respectively, higher than for the native 5% SPC/E system. This increase in the number of slow waters is due to the larger solvent accessible surface of a misfolded protein, with respect to the native state. This also follows from Fig. 3.3.7 which compares the number distributions for the native and misfolded protein as a function of decay time τ for surface waters near hydrophobic/hydrophilic groups. Similar to the native state results, both hydrophobic and hydrophilic water have a bulk like peak around 2.5 ps for the misfolded conformations. The largest difference between the native and misfolded state is the enhanced contribution of hydrophobic hydration water in the misfolded state. Not surprisingly, misfolding induces more hydrophobic residues to be exposed.

Table 3.A.3 compares the fraction of the bulk-like, moderate and slow hydration shell waters of the native and misfolded systems. The hydrophobic water in the misfolded systems exhibits a higher fraction of bulk-like water and a lower fraction of moderate and slow water compared to the native systems, and indeed, a smaller average reorientation decay time for the hydrophobic water (see Table 3.A.2). Interestingly, not only the water dynamics accelerates upon misfolding, but the hydrophobic water becomes actually slightly faster compared to the hydrophilic water. This larger fraction of non surface-perturbed waters was also observed in the work of Rahaman et al [13].

The contribution of water not H-bonded to the protein (nHB) to the decay time distributions in Fig. 3.3.7 and Figs. 3.A.5 to 3.A.10 is significantly higher for the misfolded state than for the native state. At the same time the contribution of water H-bonded to the protein (HB) only increases slightly between the native and misfolded state. This increased population of water non-H-bonded to the protein represents to a large extent the higher hydrophobic water population and similarly shows a slightly faster reorientation.

Table 3.A.1 and 3.A.2 show that the average hydration layer water in the misfolded state tends to be faster than in the native states. Water that is H-bonded to the protein remains slower than the water non-H-bonded to the protein, and as in the native systems, shows a less pronounced bulk-like peak. The H-bonded water is slightly faster in the misfolded state, unlike the H-bond lifetimes that remain unchanged. This suggests the strength of the bond does not change upon misfolding, but rather the decreased local excluded volume upon misfolding causes water to reorient faster (more bulk-like).

Interestingly, upon misfolding water that accepts a H-bond from a protein donor slightly slows down (see Table 3.A.2). In accordance with the increase of the protein donor - water H-bond lifetime (t_D, t_{Direct}) upon misfolding this bond does become stronger and therefore water reorients slower. This can be explained by the presence of water mediated H-bonds in a misfolded state (see Fig. 3.A.2). Fig. 3.3.6 shows projections of the water reorientation time on structural representations of the protein. Finally, Figs. 3.A.5 to 3.A.10 show that misfolding does not change the order of the population of H-bonding classes, but again that hydrophobic groups become more solvent accessible.

3.4 Conclusions

Using ultrafast IR spectroscopy experiments and molecular dynamics simulations we investigated the dynamics of hydration water in α-lactalbumin solutions. We found good agreement between simulation and experiment for the number of slow waters around the protein surface. We showed that the slowly reorienting water molecules are the hydration shell waters that make on average fewer H-bonds with the surrounding molecules in comparison to bulk water, in particular those waters that accept fewer H-bonds from other water molecules or protein residues. In the native state the hydrophobic water on average exhibits slightly slower reorientation dynamics than hydrophilic water. These conclusions are corroborated by experimental evidence that the slow water fraction is characterized by weaker H-bonds. The simulations show that hydration waters donating more H-bonds to their surroundings are slower, in accordance with the finding that protein H-bond accepting (hydrophilic) groups slow down reorientation.

The H-bond breaking mechanism is also affected. Near convex sites the jump process dominates the breaking procedure, while near concave sites jumping becomes less frequent, thus slowing down the reorientation of water molecules. At concave sites the diffusive process (without jumps) becomes relatively more important.

Upon misfolding a larger amount of water reorients slowly, mainly due to the increase of the solvent accessible surface. However, the hydration shell water dynamics

slightly accelerates compared to the native hydration shell water, due to an increased fraction of bulk-like waters near hydrophobic groups. In the misfolded systems, the hydrophobic residues are more exposed to the bulk and are no longer part of a concave protein cavity. As a result, the reorientation of water molecules near hydrophobic groups becomes relatively faster compared to the folded systems. The protein-water H-bond lifetime does not change significantly upon misfolding, although waters accepting a H-bond from a protein donor reorient slower, probably due to water mediated protein interactions.

Appendix

3.A Water HB and reorientation dynamics analysis.

Table 3.A.1: Simulation: Fit of the anisotropy curve for the hydration shell water population to a sum of three exponentials (eq 3.5) for the six systems of study 1) 5% SPC/E 2) 8.5% SPC/E 3) misfolded #1 4) misfolded #2 5) 5% TIP4P/2005 6) 8.5% TIP4P/2005. The number subscript indicates the error in the last digit

system #	1	2	3	4	5	6
τ_{r0}	0.20_1	0.20_1	0.19_1	0.18_1	0.21_1	0.19_1
τ_{r1}	4.56_3	4.60_4	4.39_3	4.41_3	5.47_4	5.34_4
τ_{r2}	41.08_{55}	40.8_{56}	35.12_{51}	34.44_{46}	45.35_{63}	40.20_{46}

Table 3.A.2: Simulation: Reorientation decay time τ of water molecules in ps, based on its category for the six systems of study 1) 5% SPC/E 2) 8.5% SPC/E 3) misfolded #1 4) misfolded #2 5) 5% TIP4P/2005 6) 8.5% TIP4P/2005. The number subscript indicates the error in the last digit

system #	1	2	3	4	5	6
τ_{prot}	4.07_5	4.07_4	3.85_9	3.92_6	4.93_6	5.00_6
τ_{HF}	4.02_3	4.05_5	3.98_{20}	4.09_{15}	4.80_3	4.89_5
τ_{HP}	4.17_9	4.09_4	3.75_7	3.79_3	5.17_{10}	5.22_{16}
τ_{HB}	5.05_9	5.50_{26}	4.66_{15}	4.91_{20}	6.23_{11}	6.33_{17}
τ_{nHB}	3.53_5	3.53_2	3.45_8	3.48_6	4.22_8	4.31_6
τ_{HBacc}	5.73_{15}	5.98_{26}	5.48_{22}	5.69_{26}	7.21_{14}	7.37_8
$\tau_{HBacc_{Sin}}$	6.32_{21}	6.62_{31}	5.88_{38}	6.15_2	8.25_{16}	8.21_2
τ_{HBdon}	4.25_{14}	4.65_{19}	4.42_{23}	4.74_{32}	5.11_4	5.09_{28}

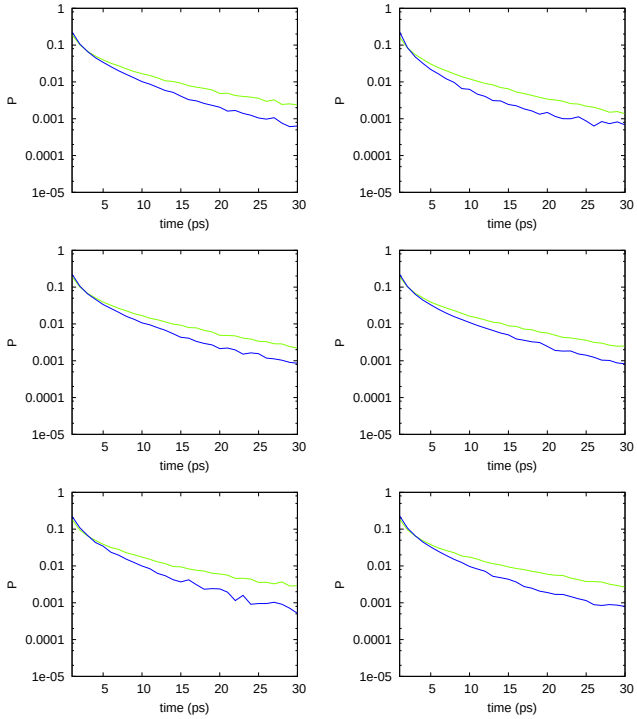

Figure 3.A.1: Simulation: Probability distribution of Protein water Hydrogen bond lifetimes for the four different systems of study a) 5% SPC/E (top left) b) 8.5% SPC/E (top right) c) misfolded #1 (middle left) d) misfolded #2 (middle right) e) 5% TIP4P/2005 (bottom left) f) 8.5% TIP4P/2005 (bottom right) . With green is highlighted the protein water hydrogen bond lifetime distribution when the protein is accepting the hydrogen from water (t_A) and blue the protein water hydrogen bond lifetime distribution when the protein is donating the hydrogen to the water (t_D)

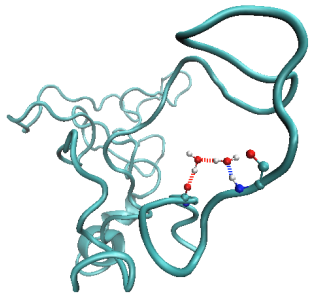

Figure 3.A.2: Water mediated protein interaction. Here we illustrate how a water of the type D is hydrogen mediating the contact of two protein residues

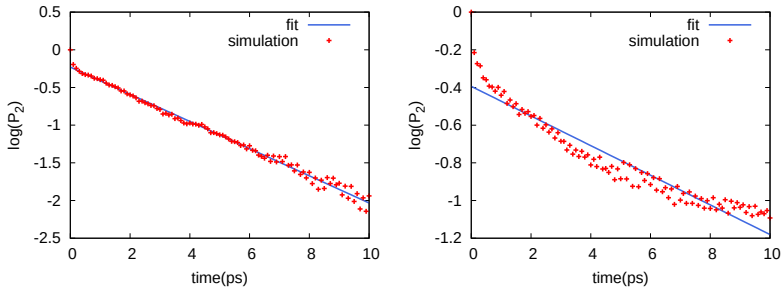

Figure 3.A.3: Simulation: Each plot depicts the reorientation decays ($log(P_2)$) of a single hydration shell water molecule from the simulation data (red) and the fitted curve (blue).

Table 3.A.3: Simulation: Fraction of hydration shell type of water molecules reorienting bulk-like, moderately slow or very slow.

	type	$\tau < 4ps$	$4 \leqslant \tau < 20ps$	$\tau \geqslant 20$
5% SPC/E	HF	0.28	0.65	0.07
	HP	0.28	0.64	0.08
	HB	0.17	0.69	0.14
	nHB	0.35	0.62	0.03
	all	0.28	0.64	0.08
8.5 % SPC/E	HF	0.28	0.65	0.07
	HP	0.30	0.62	0.08
	HB	0.18	0.67	0.15
	nHB	0.35	0.62	0.03
	all	0.29	0.64	0.07
misfolded #1	HF	0.28	0.65	0.07
	HP	0.33	0.63	0.06
	HB	0.17	0.70	0.13
	nHB	0.34	0.63	0.03
	all	0.31	0.63	0.06
misfolded #2	HF	0.28	0.65	0.07
	HP	0.32	0.62	0.06
	HB	0.21	0.67	0.12
	nHB	0.36	0.61	0.03
	all	0.30	0.63	0.07
5% TIP4P/2005	HF	0.22	0.69	0.09
	HP	0.20	0.69	0.1
	HB	0.14	0.69	0.17
	nHB	0.28	0.68	0.04
	all	0.21	0.69	0.10
8.5% TIP4P/2005	HF	0.21	0.68	0.11
	HP	0.20	0.69	0.11
	HB	0.14	0.69	0.17
	nHB	0.26	0.69	0.05
	all	0.21	0.69	0.10

Table 3.A.4: Simulation: Fraction of waters in hydration shell reorienting bulk-like, moderately slow or very slow as function number of donated and accepted H-bonds.

# donated h-bonds	$\tau < 4ps$	$4 \leqslant \tau < 20ps$	$\tau \geqslant 20$
0	0.37	0.59	0.04
1	0.32	0.62	0.06
2	0.27	0.65	0.08
# accepted h-bonds	$\tau < 4ps$	$4 \leqslant \tau < 20ps$	$\tau \geqslant 20$
0	0.20	0.64	0.16
1	0.28	0.64	0.08
2	0.30	0.64	0.06

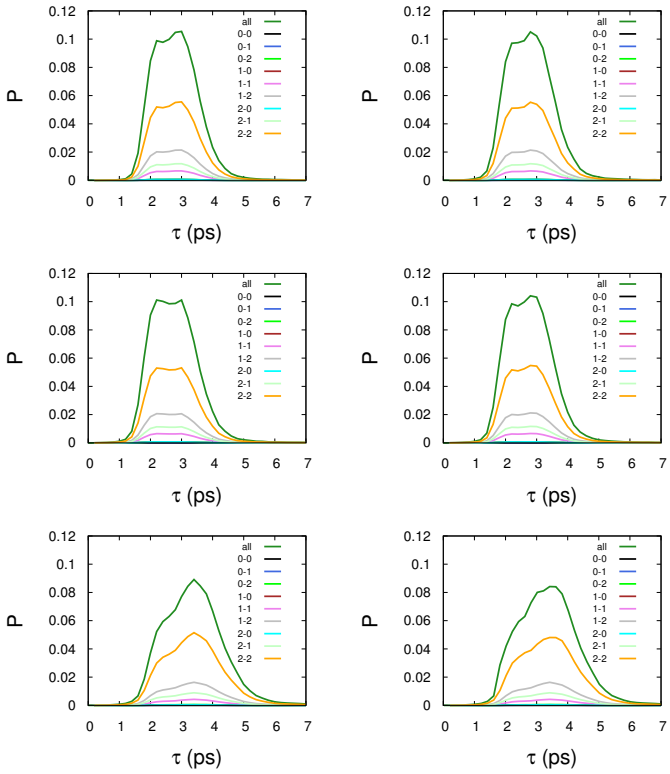

Figure 3.A.4: Simulation: Probability distribution of reorientation decay times of the bulk water for the six different systems of study for systems 5% SPC/E (top left), 8.5% SPC/E (top right), misfolding #1 (middle left), misfolding #2 (middle right), 5% TIP4P/2005 (bottom left), 8.5% TIP4P/2005 (bottom right).

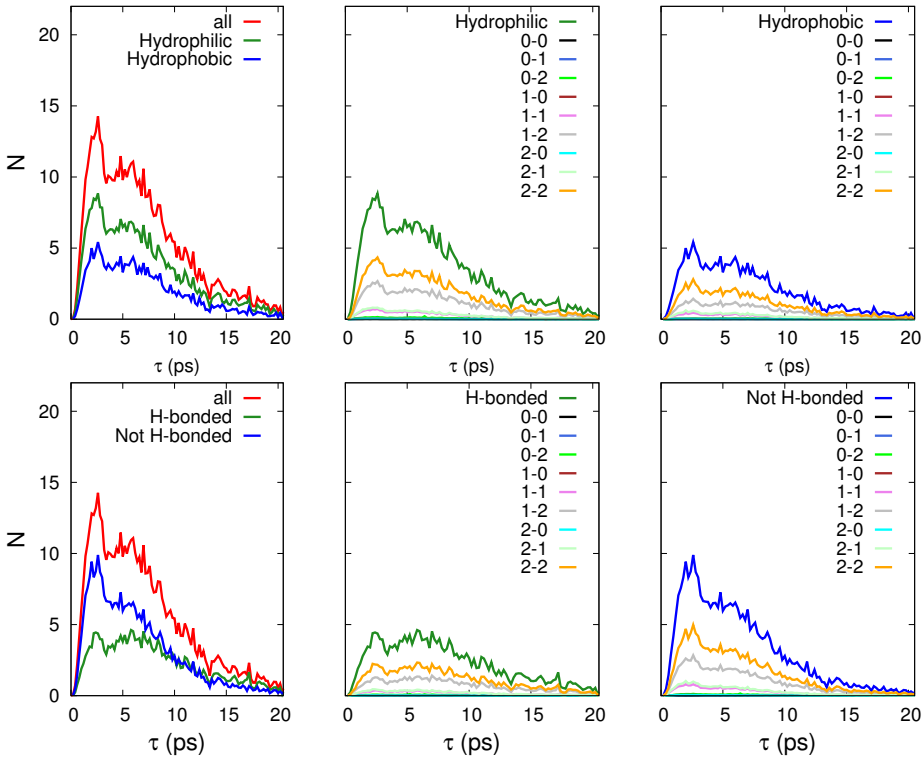

Figure 3.A.5: Simulation: Number distributions of reorientation decay times of the hydration water for 5 % SPC/E system. For the first row, the first column depicts the overall hydration water, and its subdivision into molecules hydrating hydrophilic and hydrophobic groups. The second column depicts the subdivision of hydrophilic population according to the hydrogen bond coordination. The third column depicts the subdivision of hydrophobic population according to hydrogen bond coordination. For the second row the first column depicts the overall hydration water, and subdivision into molecules that are hydrogen bonded to the protein (green) and molecules that are not (blue). The second column depicts the subdivision of h-bonded coordination according to hydrogen bond population. The third column depicts the subdivision of non-bonded population according to hydrogen bond coordination.

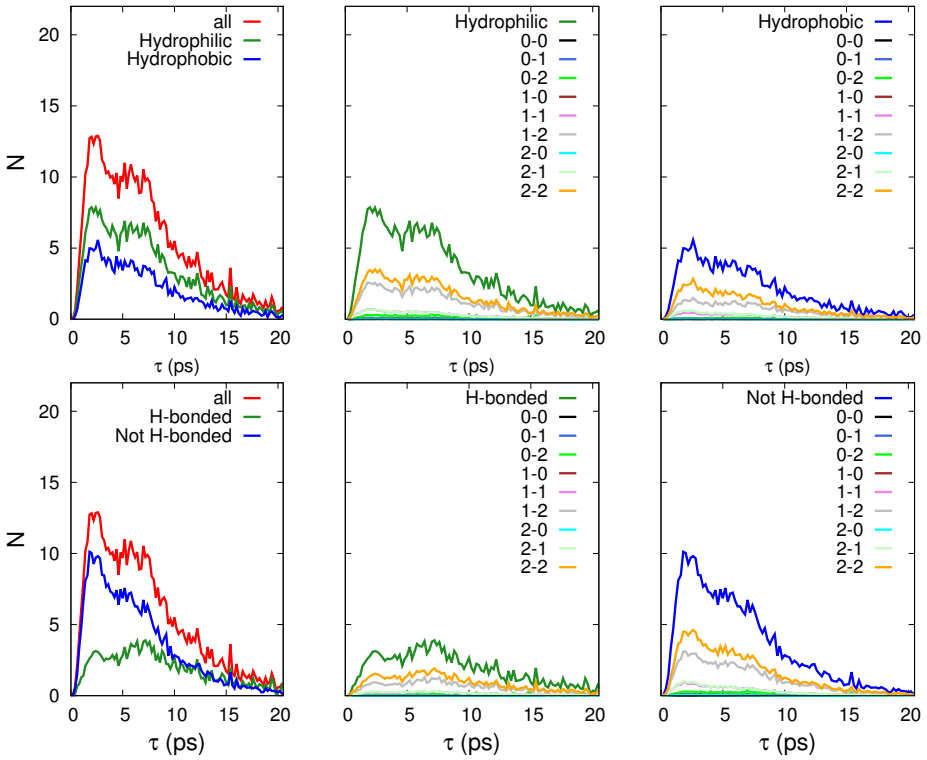

Figure 3.A.6: Simulation: Number distributions of reorientation decay times of the hydration water for 8.5 % SPC/E system. For the first row, the first column depicts the overall hydration water, and its subdivision into molecules hydrating hydrophilic and hydrophobic groups. The second column depicts the subdivision of hydrophilic population according to the hydrogen bond coordination. The third column depicts the subdivision of hydrophobic population according to hydrogen bond coordination. For the second row the first column depicts the overall hydration water, and subdivision into molecules that are hydrogen bonded to the protein (green) and molecules that are not (blue). The second column depicts the subdivision of h-bonded population according to hydrogen bond coordination. The third column depicts the subdivision of non-bonded population according to hydrogen bond coordination.

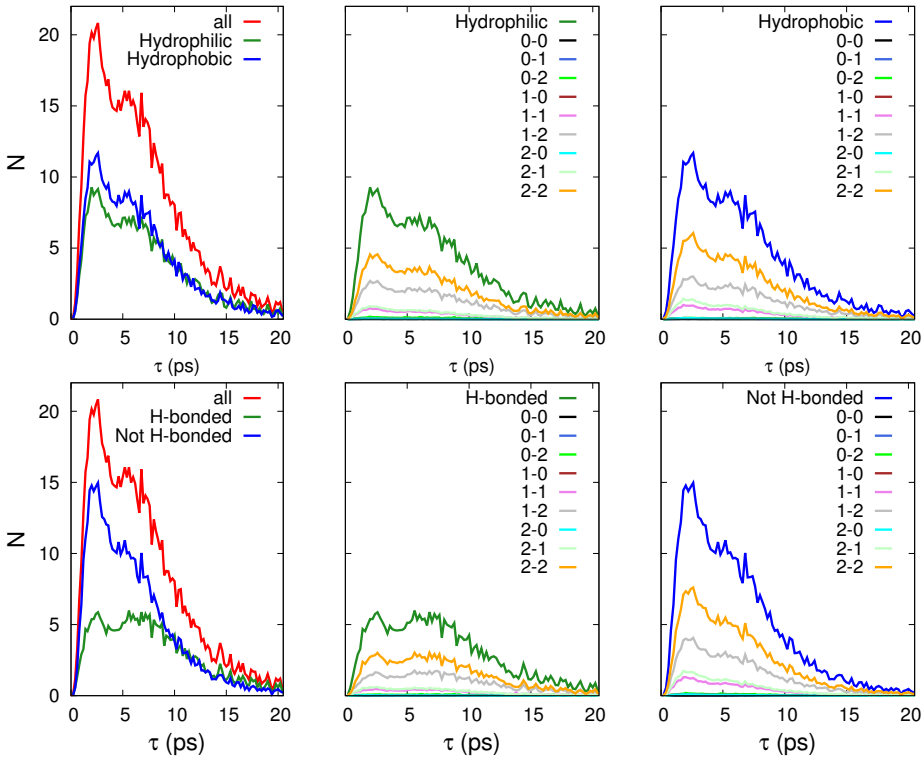

Figure 3.A.7: Simulation: Number distributions of reorientation decay times of the hydration water for the misfolded #1 system. For the first row, the first column depicts the overall hydration water, and its subdivision into molecules hydrating hydrophilic and hydrophobic groups. The second column depicts the subdivision of hydrophilic population according to the hydrogen bond coordination. The third column depicts the subdivision of hydrophobic population according to hydrogen bond coordination. For the second row the first column depicts the overall hydration water, and subdivision into molecules that are hydrogen bonded to the protein (green) and molecules that are not (blue). The second column depicts the subdivision of h-bonded population according to hydrogen bond coordination. The third column depicts the subdivision of non-bonded population according to hydrogen bond coordination.

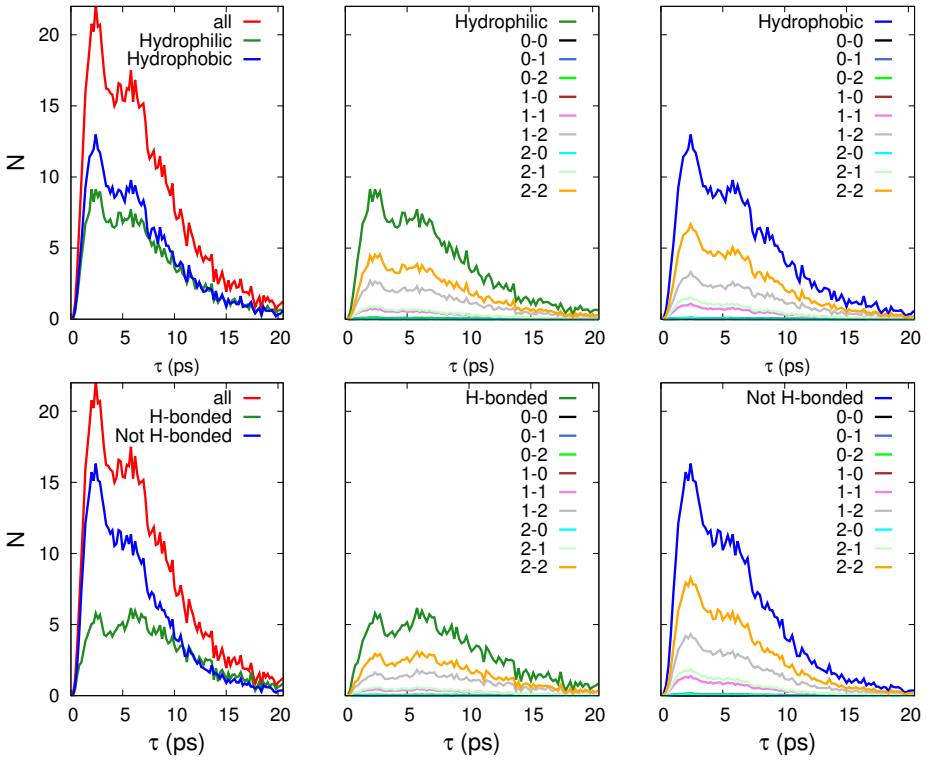

Figure 3.A.8: Simulation: Number distributions of reorientation decay times of the hydration water for the misfolded #2 system. For the first row, the first column depicts the overall hydration water, and its subdivision into molecules hydrating hydrophilic and hydrophobic groups. The second column depicts the subdivision of hydrophilic population according to the hydrogen bond coordination. The third column depicts the subdivision of hydrophobic population according to hydrogen bond coordination. For the second row the first column depicts the overall hydration water, and subdivision into molecules that are hydrogen bonded to the protein (green) and molecules that are not (blue). The second column depicts the subdivision of h-bonded population according to hydrogen bond coordination. The third column depicts the subdivision of non-bonded population according to hydrogen bond coordination.

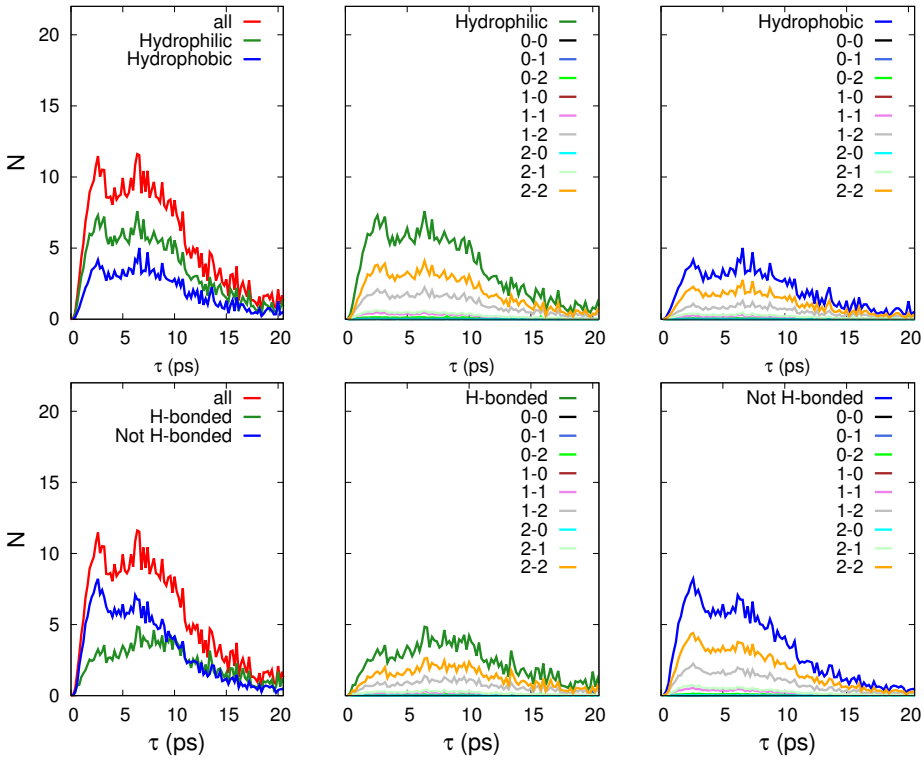

Figure 3.A.9: Simulation: Number distributions of reorientation decay times of the hydration water for 5.5 % TIP4P/2005 system. For the first row, the first column depicts the overall hydration water, and its subdivision into molecules hydrating hydrophilic and hydrophobic groups. The second column depicts the subdivision of hydrophilic population according to the hydrogen bond coordination. The third column depicts the subdivision of hydrophobic population according to hydrogen bond coordination. For the second row the first column depicts the overall hydration water, and subdivision into molecules that are hydrogen bonded to the protein (green) and molecules that are not (blue). The second column depicts the subdivision of h-bonded population according to hydrogen bond coordination. The third column depicts the subdivision of non-bonded population according to hydrogen bond coordination.

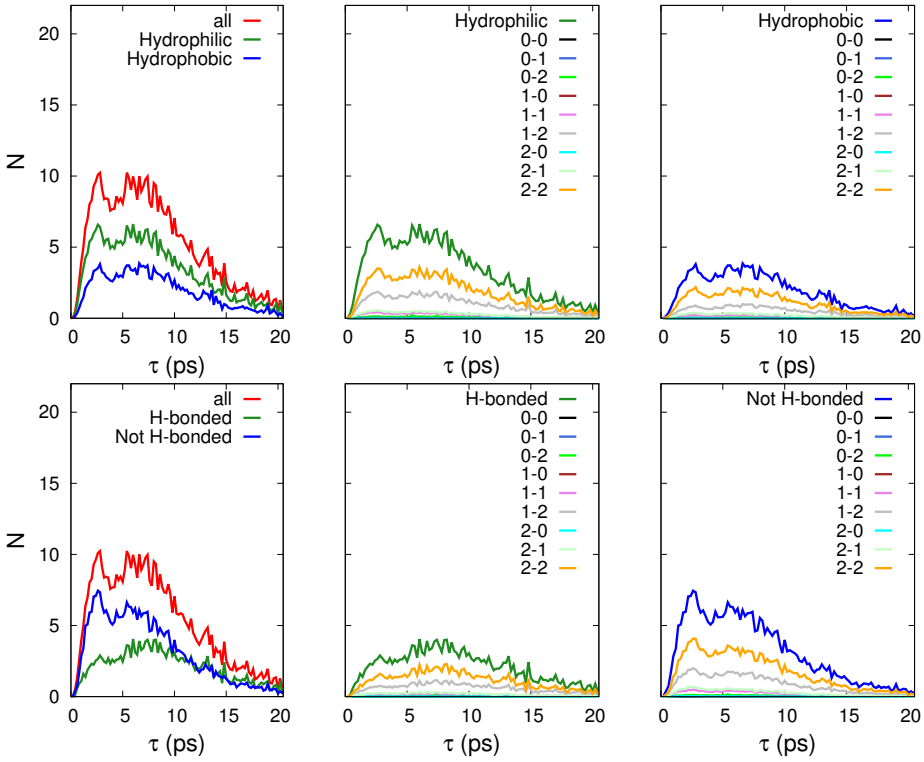

Figure 3.A.10: Simulation: Number distributions of reorientation decay times of the hydration water for 8.5 % TIP4P/2005 system. For the first row, the first column depicts the overall hydration water, and its subdivision into molecules hydrating hydrophilic and hydrophobic groups. The second column depicts the subdivision of hydrophilic population according to the hydrogen bond coordination. The third column depicts the subdivision of hydrophobic population according to hydrogen bond coordination. For the second row the first column depicts the overall hydration water, and subdivision into molecules that are hydrogen bonded to the protein (green) and molecules that are not (blue). The second column depicts the subdivision of h-bonded coordination according to hydrogen bond coordination. The third column depicts the subdivision of non-bonded population according to hydrogen bond coordination.

Bibliography

[1] S. Bandyopadhyay, S. Chakraborty, and B. Bagchi, J. Am. Chem. Soc. **127**, 16660 (2005).

[2] R. K. Eppler, R. S. Komor, J. Huynh, J. S. Dordick, J. A. Reimer, and D. S. Clark, Proc. Natl. Acad. Sci. U.S.A. **103**, 5706 (2006).

[3] M. Grossman, B. Born, M. Heyden, D. Tworowski, G. B. Fields, I. Sagi, and M. Havenith, Nat. Struct. Mol. Biol. **18**, 1102 (2011).

[4] S. Kiihne and R. G. Bryant, Biophys. J. **78**, 2163 (2000).

[5] F. Sterpone, G. Stirnemann, and D. Laage, J. Am. Chem. Soc. **134**, 4116 (2012).

[6] T. Li, A. A. Hassanali, Y.-T. Kao, D. Zhong, and S. J. Singer, J. Am. Chem. Soc. **129**, 3376 (2007).

[7] D. Fogarty, Aoife C and Laage, J Phys Chem B **118**, 7715 (2014).

[8] B. Halle, Philos Trans R Soc Lond B Biol Sci **359**, 1207 (2004).

[9] A. M. Dokter, S. Woutersen, and H. J. Bakker, Proc. Natl. Acad. Sci. U.S.A. **103**, 15355 (2006).

[10] E. E. Fenn, D. B. Wong, and M. D. Fayer, Proc. Natl. Acad. Sci. U.S.A. **106**, 15243 (2009).

[11] A. A. Bakulin, M. S. Pshenichnikov, H. J. Bakker, and C. Petersen, J. Phys. Chem. A **115**, 1821 (2011).

[12] J. C. Jose, P. Khatua, N. Bansal, N. Sengupta, and S. Bandyopadhyay, J. Phys. Chem. B **118**, 11591 (2014).

[13] O. Rahaman, S. Melchionna, D. Laage, and F. Sterpone, Phys. Chem. Chem. Phys **15**, 3570 (2013).

[14] C. R. Markus, B. Olivier, G. E. M. Panhuysen, J. V. D. Gugten, M. S. Alles, A. Tuiten, H. G. M. Westenberg, D. Fekkes, H. F. Koppeschaar, and E. E. H. F. D. Haan, Am J Clin Nutr **71**, 1536 (2000).

[15] O. y. Halskau, R. Perez-jimenez, B. Ibarra-molero, J. Underhaug, V. Mun, A. Martinez, and J. M. Sanchez-ruiz, Proc. Natl. Acad. Sci. U.S.A. **105**, 8625 (2008).

[16] S. Pronk, S. Páll, R. Schulz, P. Larsson, P. Bjelkmar, R. Apostolov, M. R. Shirts, J. C. Smith, P. M. Kasson, D. van der Spoel, et al., Bioinformatics (Oxford, England) **29**, 845 (2013).

[17] E. D. Chrysina, K. Brew, and K. R. Acharya, J. Biol. Chem. **275**, 37021 (2000).

[18] K. Lindorff-Larsen, S. Piana, K. Palmo, P. Maragakis, J. L. Klepeis, R. O. Dror, and D. E. Shaw, Proteins **78**, 1950 (2010).

[19] G. Bussi, D. Donadio, and M. Parrinello, J. Chem. Phys. **126**, 014101 (2007).

[20] M. Parrinello, J. Appl. Phys. **52**, 7182 (1981).

[21] I.-c. Lin, A. Seitsonen, I. Tavernelli, and U. Rothlisberger, J. Chem. Theory Comput. **8**, 3902 (2012).

[22] H. J. C. Berendsen, J. P. M. Postma, W. F. Van Gunsteren, and J. Hermans, *Intermolecular Forces, ed Pullman B* (1981).

[23] J.-B. Brubach, A. Mermet, A. Filabozzi, A. Gerschel, and P. Roy, J. Chem. Phys. **122**, 184509 (2005).

[24] W. H. Brandeburgo, T. V. D. Post, and J. Meijer, Phys. Chem. Chem. Phys. **17**, 24968 (2015).

[25] H. J. Bakker and J. L. Skinner, Chem Rev **110**, 1498 (2010).

[26] G. Lipari and A. Szabo, Biophys J **30**, 489 (1980).

[27] F. Massi and J. E. Straub, J. Comput. Chem. **24**, 143 (2003).

[28] Y. Rezus and H. Bakker, Phys. Rev. Lett. **99**, 148301 (2007).

[29] T. H. van der Loop, M. R. Panman, S. Lotze, J. Zhang, T. Vad, H. J. Bakker, W. F. C. Sager, and S. Woutersen, J. Chem. Phys. **137**, 044503 (2012).

[30] S. T. van der Post and H. J. Bakker, Phys. Chem. Chem. Phys. **14**, 6280 (2012).

[31] Z. F. Brotzakis, C. C. M. Groot, W. H. Brandeburgo, H. J. Bakker, and P. G. Bolhuis, J Phys Chem B **120**, 4756 (2016).

[32] F. Sterpone, G. Stirnemann, J. T. Hynes, and D. Laage, J. Phys. Chem. B. **114**, 2083 (2010).

[33] G. Pabón and L. M. Amzel, Universitas Scientiarum **17**, 273 (2012).

[34] D. Laage and J. T. Hynes, Science **311**, 832 (2006).

[35] C. Vega and J. L. F. Abascal, Phys. Chem. Chem. Phys. **13**, 19663 (2011).

[36] K. Usui, J. Hunger, M. Sulpizi, T. Ohto, M. Bonn, and Y. Nagata, J. Phys. Chem. B. **119**, 10597 (2015).

[37] B. Auer and J. Skinner, Chem. Phys. Lett. **470**, 13 (2009).

[38] H. Xu, H. Stern, and B. Berne, J. Phys. Chem. B. **25**, 2054 (2002).